Biointerface Research in Applied Chemistry
Platinum Open Access Journal (ISSN: 2069-5837)

Article
Volume 12, Issue 6, 2022, 7972 - 7982
https://doi.org/10.33263/BRIAC126.79727982

Performance Optimization of Sulfur Dioxide (SO_2) Desulfurization by Oil Palm-based Activated Carbon Using Box-Behnken Design

S. Kathiroly Sooriyan [1], Naimah Ibrahim [1,*], Muhammad Adli Hanif [1], Masitah Hasan [1], Sureena Abdullah [2], Agus Aan Adriansyah [3], Budhi Setianto [3], Achmad Syafiuddin [3]

[1] Water Research and Environmental Sustainability Growth (WAREG), Faculty of Civil Engineering Technology, Universiti Malaysia Perlis, 02600 Arau, Perlis, Malaysia
[2] Faculty of Chemical and Natural Resources Engineering, University Malaysia Pahang (UMP), Pahang, Malaysia
[3] Department of Public Health, Universitas Nahdlatul Ulama Surabaya, 60237 Surabaya, Indonesia
* Correspondence: naimah@unimap.edu.my (N.I.);

Scopus Author ID 23767004300
Received: 1.10.2021; Revised: 15.11.2021; Accepted: 17.11.2021; Published: 5.12.2021

Abstract: Sulfur dioxide (SO_2) emission into the atmosphere brought by the burning of fossil fuels in the industries posed significant negative effects on the environment and human beings. Adsorption using activated carbon from agricultural wastes is a viable method commonly used to counter this major problem. SO_2 breakthrough experiment was conducted on a fixed bed reactor using oil palm empty fruit bunch activated carbon. The sorbent utilized in this study was characterized via N_2 adsorption-desorption isotherm, field emission scanning electron microscopy, and Fourier transform infrared spectroscopy. Three parameters, i.e., reaction temperature, inlet SO_2 concentration, and adsorbent dosage, were optimized using Box-Behnken Design. The highest SO_2 removal was obtained at 70 °C, 2000 ppm of SO_2, and 1 g of adsorbent with adsorption capacity of approximately 1101 mg SO_2/g activated carbon. The developed model was validated using Analysis of Variance (ANOVA), and good agreement between predicted and actual values was obtained. Inlet SO_2 concentration, adsorbent dosage, the interaction between these two parameters, and all quadratic terms were found to be significant factors, with adsorbent dosage being most significant based on its highest F-value.

Keywords: activated carbon; response surface method; box-Behnken design; optimization; SO_2 removal.

1. Introduction

Despite the current enhancement of green and renewable technology, most industries are still dependent on the usage of fossil fuels as a source of energy due to their high energy density. The combustion of fossil fuels releases sulfur dioxide (SO_2) gas into the atmosphere. SO_2 emitted can be carried over long distances due to its long residence time (3-5 days), depending on the meteorological conditions. SO_2 is known as the precursor of acid rain, resulting in acidification of water bodies, damage of crops, corrosion of buildings, etc. [1]. Additionally, its effect on human beings has also been reported, including difficulties in respiration, pulmonary function changes, and worsening cardiovascular diseases [2].

An adsorption is a viable option in mitigating SO_2 emission problems due to its efficiency, simplicity, economic and possible adsorbent regeneration [3]. Activated carbon synthesized from agricultural waste is commonly utilized to solve two environmental problems

simultaneously, i.e., emission of gaseous pollutants and disposal of agricultural waste. Palm oil milling is one of the major agricultural processes in Malaysia, where for every ton of fresh fruit bunch processed, 22 % of the waste generated is an empty fruit bunch (EFB) [4]. EFB is an agricultural waste with very low commercial value, and the excessive amount discarded may pose significant environmental issues. The use of EFB as an activated carbon precursor for various gaseous pollutants adsorption such as carbon monoxide (CO), nitric oxide (NO), and hydrogen sulfide (H_2S) has been successfully reported by several studies [5–7]. To our best knowledge, the use of oil palm waste as an activated carbon precursor for SO_2 desulfurization has been largely focused on the palm kernel shell; thus, the use of EFB as an alternative is highly appealing.

Optimization of reaction parameters is an important step in desulfurization studies to obtain the best adsorption capacity and removal efficiency with the ideal usage of energy and resources. Response Surface Methodology (RSM) is a statistical and mathematical representation of a response plotted as a function of the input variables used to develop, improvise, and optimize a process. The response obtained by RSM considered center points and edge or face center points of the process, which consequently will provide a better model of the response variable [8]. Box-Behnken Design (BBD) is an example of a commonly used RSM design that uses three-level designs, a combination of 2k factorial designs with incomplete block designs [9]. The advantage of this method is the exclusion of all corner points and star points in the design. The response obtained in this design is never higher or lower than the maximum and the minimum value assigned. Compared to other RSM designs, BBD requires fewer center points as the points on the edges are closer to the middle, thus resulting in fewer overall experimental runs needed [8].

This study focuses on optimizing SO_2 desulfurization on activated carbon originated from oil palm empty fruit bunch (EFBAC). The sorbent was characterized via nitrogen (N_2) adsorption-desorption isotherm, field emission scanning electron microscopy, and Fourier transform infrared spectroscopy to understand their physical and chemical properties. Three reaction parameters, e.g., reaction temperature, inlet SO_2 concentration, and adsorbent dosage, are optimized via Box-Behnken Design to develop a model that correlates the three parameters using a second-degree polynomial equation. The developed model will be verified using Analysis of Variance (ANOVA) to determine the validity of the model, the significance of each parameter, and the interaction between them.

2. Materials and Methods

2.1. Sample preparation.

Oil palm EFB used in this study was collected from a palm mill factory located in Nibong Tebal, Penang, Malaysia. EFB fibers were thoroughly cleaned to remove any impurities and oven-dried at 110 °C before the activation process. Activated carbon was prepared by soaking raw EFB with concentrated phosphoric acid (H_3PO_4) at 1:4 (wt./vol.) followed by carbonization at 500 °C for 2 hours. The carbonized sample was cooled to room temperature and intensively washed with distilled water until neutral pH was attained to remove any excess acid present and oven-dried overnight at 110 °C. The dried sample was crushed and sieved, and powdered particles with a size between 300-600 μm were utilized in this study.

2.2. Characterization.

The surface area and porosity of EFBAC were determined using N_2 adsorption-desorption using Belsorp Mini II at – 196 °C. Before measurement, the samples were degassed at 120 °C for 3 hours. The samples' surface area and average pore size were determined by Brunauer-Emmett-Teller (BET) analysis and Barrett-Joyner-Halenda (BJH) model, respectively. The pore volume was determined by calculating the adsorbed N_2 volume at standard temperature and pressure (STP). Field emission scanning electron microscopy (FESEM) was utilized to determine the surface morphology of the prepared EFBAC using FEI Nova NanoSEM 450. The sample was coated with a platinum coating to improve the sample imaging, and the images were captured at a magnification of x5000. The surface chemistry of EFBAC was analyzed by Fourier transform infrared spectroscopy (FTIR) using Perkin Elmer Spectrum 65 FTIR in the mid-range IR wavelength of 4000 – 450 cm^{-1} . The spectra obtained were compared with available FTIR databases or any related studies to identify the functional groups present.

2.3. SO_2 Removal.

SO_2 breakthrough experiment was conducted on a lab-scale fixed-bed quartz reactor (l = 25 cm, ID = 8.8 mm) using special mix gas of 0.3 % SO_2/N_2. The reaction temperature and inlet SO_2 concentration were controlled by a tubular furnace and mass flow controller, respectively. The sample was pre-treated with nitrogen (N_2) gas at 150 °C for 1 hour prior to each breakthrough experiment to remove any impurities. The reactor was then cooled down to the desired reaction temperature. Once the temperature became stable, the simulated flue gas was passed through the reactor, and the outlet concentration was continuously measured using a multigas gas analyzer (Testo 340) equipped with an electrochemical SO_2 gas sensor.

The adsorption capacity of the sample was calculated at $C/C_0 = 0.95$ using the following equation [10], where q is adsorption capacity (mg/g), C_0 and C_A is SO_2 concentration at the inlet and at a specific time (mg/L), respectively; Q_f is the gas flow rate (L/min), y_t is a gas molar fraction, and m_c is mass of the activated carbon (g).

$$q = \frac{C_0 Q_f y_t}{m_c} \int_0^{\infty} 1 - \frac{C_A}{C_0}\, dt \qquad (1)$$

Reaction parameters, i.e., temperature (A), inlet SO_2 concentration (B), and adsorbent dosage (C), were optimized using Box-Behnken Design (BBD) with the aid of Design-Expert Software Version 11. The minimum (-1), center (0), and maximum (1) levels for the three variables were selected based on literature, preliminary studies, and instrumental limitations. The values are shown in Table 1.

Table 1. Independent variables matrix and encoded levels for BBD.

Independent variables	Code	Levels		
		-1	0	1
Temperature (°C)	A	40	70	100
Inlet SO_2 concentration (ppm)	B	1250	1625	2000
Adsorbent dosage (g)	C	1	2.5	4

SO_2 adsorption capacity obtained from the suggested 15 experimental runs as the response variable was used to develop an empirical, quadratic model which correlates the three independent variables using the second-degree polynomial equation as shown below [11],

where Y, β, and ε are the response variable, regressors, and the statistical error term, respectively.

$$Y = \beta_0 + \beta_1 A + \beta_2 B + \beta_3 C + \beta_{12} AB + \beta_{13} AC + \beta_{23} BC + \beta_{11} A^2 + \beta_{22} B^2 + \beta_{33} C^2 + \varepsilon \quad (2)$$

The significance of the model developed, and the interaction between the independent variables was determined using Analysis of Variance (ANOVA) by analyzing the correlation coefficient value (R^2), Fisher value (F-value), and probability (p-value). A larger magnitude of F-value and a smaller p-value implies the level of significance of the corresponding coefficients. P-value < 0.05 is required to indicate significant regression and a good correlation between predicted and experimental results.

3. Results and Discussion

3.1. Sample characterization.

N_2 adsorption-desorption isotherm of EFBAC shown in Figure 1 exhibits a Type IV(a) isotherm with H4 hysteresis loop, indicating a sorbent with microporous-mesoporous nature with the hysteresis accompanies the phenomenon of capillary condensation [12]. The EFBAC utilized in this study possesses a surface area of 437.88 m^2/g, a total pore volume of 0.3077 cm^3/g, an average pore diameter of 2.811 nm, and the highest N_2 uptake of 200.8 cm^3/g. These properties are significantly greater than other sorbents reported for the SO_2 desulfurization study. The chemical activation by H_3PO_4 resulted in the linkage between phosphate and polyphosphate esters that protect internal pore structure and avoid excessive burn off leading to higher surface area and greater formation of mesopores.

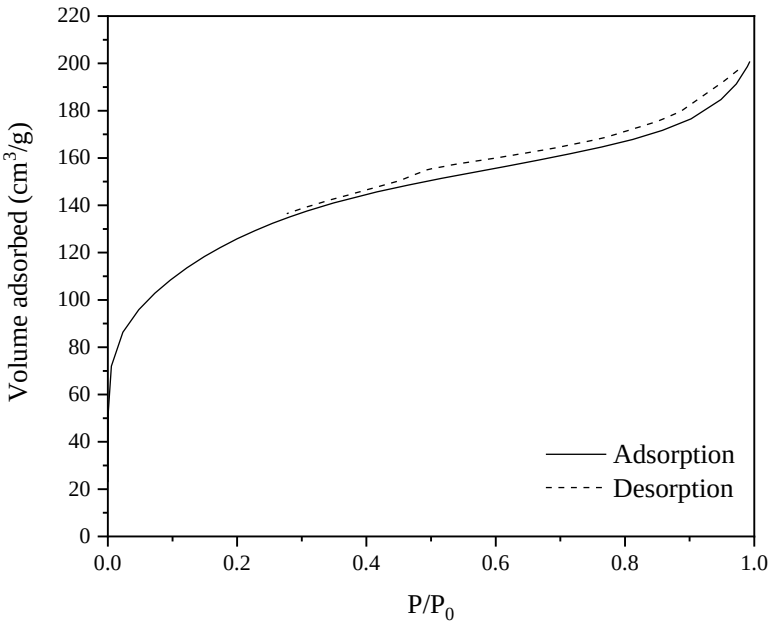

Figure 1. N_2 adsorption-desorption isotherm of EFBAC.

The combination of micropores and mesopores of EFBAC is further validated by the surface morphology shown in Figure 2. The pore diameter is in the range of 0.23 – 19.44 μm, and the majority of the pores are mesopores (> 2 μm). This implied that the chemical activation

and heat treatment conducted on EFBAC has successfully resulted in pore development, critical during a desulfurization process.

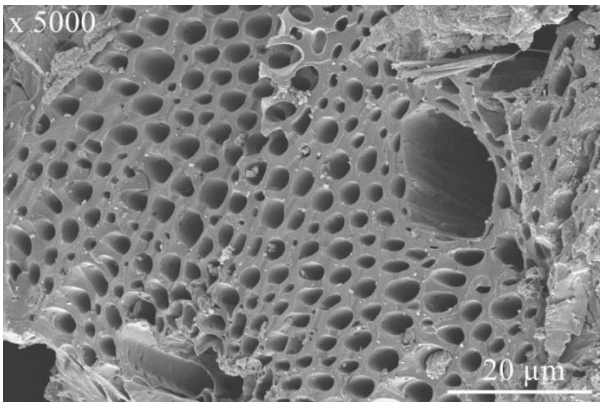

Figure 2. Surface morphology of EFBAC (Magnification: x5000).

FTIR spectra of EFBAC in the range between 4000 – 450 cm^{-1} are shown in Figure 3. The results obtained were compared and matched with the available FTIR database and spectra from previous studies. Chemical activation by H_3PO_4 has incremented groups like acidic and phenolic hydroxyl, carboxyl, and phosphate on the carbon surface. The broad curve within 3600 – 3200 cm^{-1} represents the hydroxyl functional groups' O–H stretching vibration mode due to adsorbed moisture content [13]. Two minor peaks observed between 2900 – 2800 cm^{-1} can be ascribed to C–H vibrations in alkanes and alkyls [13,14]. Shallow peaks around 2400 – 2200 cm^{-1} can be assigned to C≡C vibrations in the alkyne and methylene group or possible C≡N stretching [15,16]. The peak between 1720 – 1700 $cm^{-1,}$ which is overlapped and merged with larger peaks, can be designated to the carboxylic acid group (C=OOH).

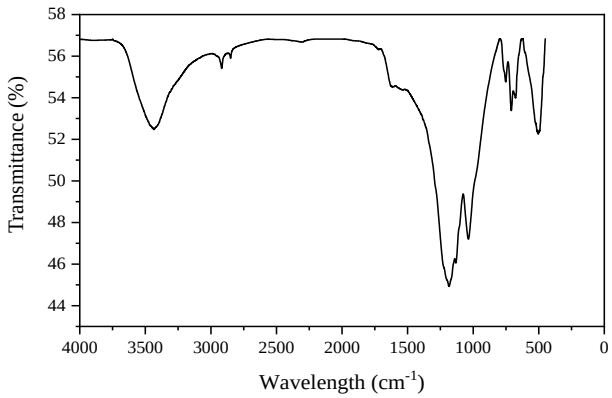

Figure 3. FTIR spectra of EFBAC.

The most prominent peak can be observed between 1350 – 750 cm^{-1} which consists predominantly of acidic oxygenated carbon groups due to H_3PO_4 activation of the EFB precursor. The oxidized carbon groups, e.g., ether, esters, carboxyl, phenolic, etc., are represented by the long peak at 1250 – 1150 cm^{-1} [17,18]. This peak can also be assigned to P–OOH group, the linkage between P–O in phosphate/polyphosphate with O–C stretching in the P–O–C linkage or hydrogen-bonded P=O due to the chemical activation by H_3PO_4 [14], [17]. The narrow and sharp peak at 1050 cm^{-1} can be attributed to the presence of C–OH or =C–OH stretching [15,19], while multiple peaks observed between 715 – 670 cm^{-1} can be assigned to the out-of-plane C-H bond of the aromatic ring [15]. A single peak at 530 – 480 cm^{-1} represents aromatic structures or P−C phosphorus-containing compounds [20].

3.2. Process optimization.

The complete design matrix of 15 experimental runs suggested by BBD and their respective responses (SO_2 adsorption capacity) are presented in Table 2. The empirical model which exhibits the relationship between the three parameters studies and SO_2 adsorption capacity obtained in coded factors is expressed in Equation 2, where A, B, and C represent reaction temperature, inlet SO_2 concentration, and sorbent dosage, respectively.

$$Y = 220.485 + 7.648A + 0.876B - 162.590C + 0.001AB - 0.062AC + 0.136BC - 0.061A^2 - 0.001B^2 - 36.592C^2 \quad (2)$$

Table 2. Experimental design matrix for optimization of SO_2 desulfurization.

Run	A: Temperature (°C)	B: Inlet SO_2 concentration (ppm)	C: Adsorbent dosage (g)	Response
1	100	1625	4	705.41
2	100	1625	1	1082.8
3	70	1625	2.5	1015.8
4	40	1625	1	1066.8
5	70	2000	1	1101.3
6	40	2000	2.5	996.37
7	70	1250	4	542.43
8	40	1625	4	700.45
9	70	1625	2.5	1035.9
10	70	1250	1	1096.7
11	100	1250	2.5	837.55
12	70	2000	4	852.97
13	70	1625	2.5	1026.5
14	40	1250	2.5	836.46
15	100	2000	2.5	1033.0

The relationship between actual experimental results and predicted values was determined by regression analysis by comparing the value of R^2 obtained (0.9979 vs. 0.9733) as shown in Fig 2. This result implies that the predicted adsorption capacity is in good agreement with actual experimental values obtained.

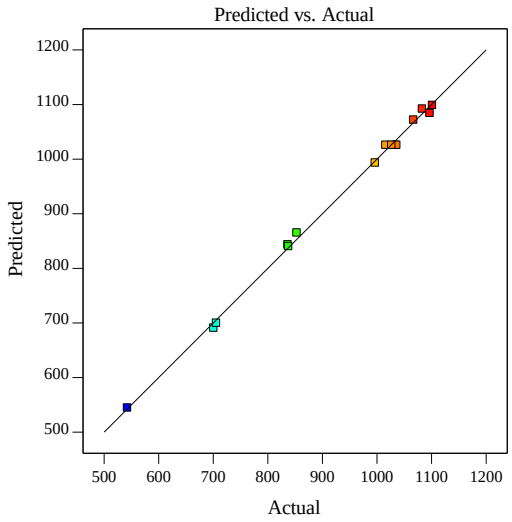

Figure 4. Predicted and actual values of SO_2 adsorption capacity on EFBAC.

The adequacy of the model was further evaluated using ANOVA, and the data is presented in Table 3. The quadratic model obtained is significant with an F-value of 265.42 and a p-value of < 0.0001. Independent effects of inlet SO_2 concentration (B) and adsorbent dosage (C) and synergistic effects between these two variables (AB) are also proven to be

significant. Additionally, all quadratic terms (A^2, $B^{2,}$ and C^2) are significant model terms. Among these factors, adsorbent dosage poses the most significant effect with the highest F-value of 1709.15. The order of significance among the model terms is: C > B > C^2 > BC > A^2 > B^2. This model's "Lack-of -Fit" was not significant, which implies that the developed quadratic model fits well.

Table 3. ANOVA Analysis of optimization of SO_2 desulfurization reaction parameters.

Source	Sum of squares	DF	Mean square	F-value	P-value	
Model	4.178 x 10^{-5}	9	46417	265.4	< 0.0001	Significant
A	430.6	1	430.6	2.460	0.1774	
B	56179	1	56179	321.2	< 0.0001	
C	2.989 x 10^{-5}	1	2.989 x 10^{-5}	1709	< 0.0001	
AB	315.3	1	315.3	1.800	0.2371	
AC	30.67	1	30.67	0.1754	0.6927	
BC	23408	1	23409	133.9	< 0.0001	
A^2	11107	1	11107	63.51	0.0005	
B^2	7595	1	7595	43.43	0.0012	
C^2	25029	1	25029	143.1	< 0.0001	
Residual	874.4	5	174.9			
Lack of Fit	670.9	3	223.6	2.200	0.3279	Not significant
Pure Error	203.5	2	101.7			
Cor Total	4.186 x 10^{-5}	14				

The effects of the three interacting factors (AB, AC, and BC) on SO_2 removal can be represented by three-dimensional (3D) contour models. The 3D model related to temperature is shown in Figures 4 and 5 for interaction with inlet SO_2 concentration (AB) and sorbent dosage (AC), respectively. From both figures, it can be observed that the adsorption capacity obtained at different reaction temperatures with constant inlet SO_2 concentration and sorbent dosage are quite similar, albeit the performance at 70 °C is slightly higher. The adsorption capacity was increased by using higher SO_2 concentrations and fewer sorbents.

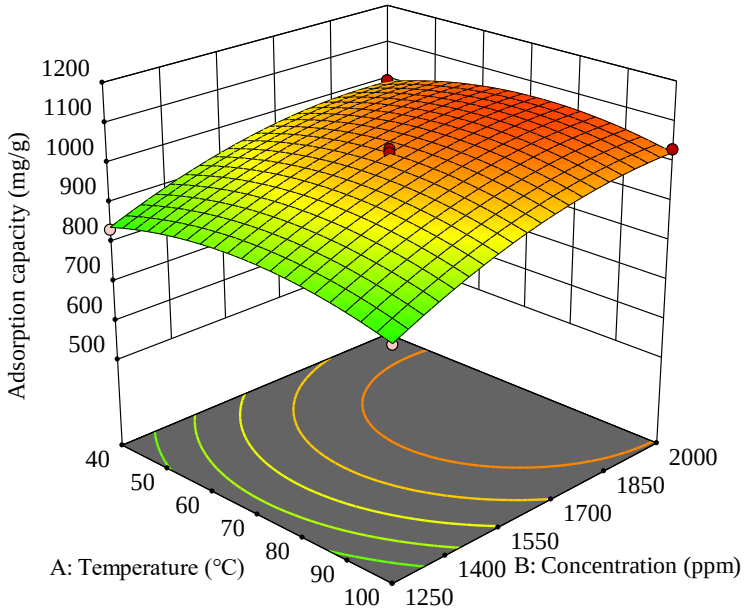

Figure 5. 3D contour plot of interaction between temperature and inlet SO_2 concentration.

The insignificance of the reaction temperature in the developed model is unprecedented as SO2 desulfurization is an exothermic process and favors lower temperatures. However, most studies on the significance of temperature were typically conducted at constant SO_2 concentration and adsorbent dosage; thus, the effect of temperature appears to be very prevalent

[21,22]. In this study, all three parameters were varied throughout the experimental runs. It can be concluded that the effect of temperature is not significant in the range tested (40-100 °C) compared to the effect brought by the other two factors.

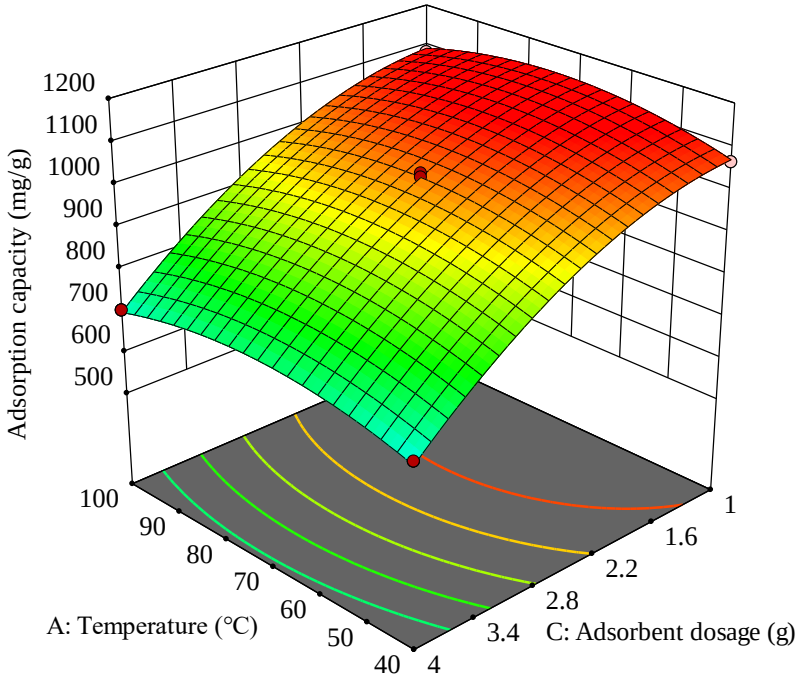

Figure 6. 3D contour plot of interaction between temperature and sorbent dosage.

A synergistic effect was expected between inlet SO_2 concentration and adsorbent dosage as various studies have reported this phenomenon. Figure 6 and Figure 7 show 3D contour plot of SO_2 adsorption capacity with a variation of these two parameters. An increment of inlet concentration often enhances adsorption capacity as a greater number of SO_2 molecules lead to enhancement of diffusion driving force and sorption capacity [23].

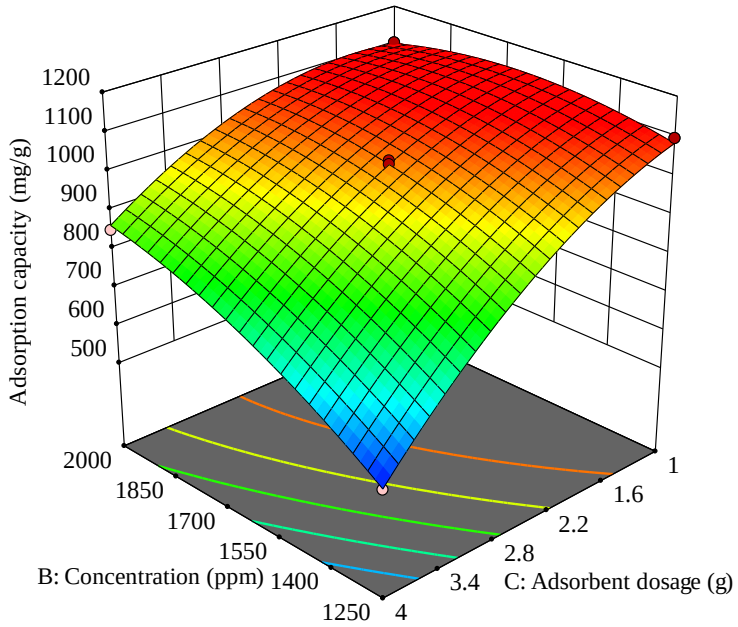

Figure 7. 3D contour plot of interaction between inlet SO_2 concentration and sorbent dosage.

Nonetheless, sorbent also plays a critical role in providing the available active sites for the adsorption process. Low sorbent dosage/SO_2 concentration ratio became the limiting factor,

resulting in adsorbent bed quick saturation, shorter breakthrough time, and lower removal efficiency. Conversely, excessive sorbent dosage/SO_2 concentration ratio results in wastage of sorbent and unoptimized removal capacity due to insufficient gas molecules to be adsorbed [24-29]. Based on Figure 7, the highest adsorption capacity was obtained at an inlet SO_2 concentration of 2000 ppm and sorbent dosage of 1 g.

4. Conclusions

SO_2 desulfurization using oil palm empty fruit bunch-based activated carbon was optimized by developing a quadratic model using Response Surface Method with Box-Behnken Design, where good agreement was attained between predicted and experimental results. The model developed and independent variables, i.e., inlet SO_2 concentration and adsorbent dosage were significant in improving SO_2 adsorption capacity. The effect of adsorbent dosage was the most significant with an F-value of 1709.15, while the order of significance is in the order of $C > B > C^2 > BC > A^2 > B^2$. The only interaction between inlet SO_2 concentration and adsorbent dosage was found significant in enhancing adsorption capacity. The optimized condition was obtained at a reaction temperature of 70 °C, inlet SO_2 concentration of 2000 ppm, and adsorbent dosage of 1 g. Reaction temperature, which was expected to play a significant role in SO_2 removal, was found to be on the contrary, possibly due to the range of temperature tested only causing small effects compared to the other two independent factors.

Funding

This research received no external funding.

Acknowledgments

The authors are deeply thankful to the local palm oil mill, which provided their empty palm fruit as raw material for activated carbon preparation.

Conflicts of Interest

All authors certify that they have no affiliations with or involvement in any organization or entity with any financial interest or non-financial interest in the subject matter or materials discussed in this manuscript.

References

1. Meimand, M.M.; Javid, N.; Malakootian, M. Adsorption of sulfur dioxide on clinoptilolite/nano iron oxide and natural clinoptilolite. *Heal Scope* **2019**, *8*, https://doi.org/10.5812/jhealthscope.69158.
2. WHO Air quality guidelines for particulate matter, ozone, nitrogen dioxide and sulfur dioxide. https://apps.who.int/iris/handle/10665/69477 (accessed on 30 July **2021**)
3. Davarnejad, R.; Panahi, P. Cu(II) removal from aqueous wastewaters by adsorption on the modified Henna with Fe_3O_4 nanoparticles using response surface methodology. *Sep Purif Technol* **2016**, *158*, 286–292, https://doi.org/10.1016/j.seppur.2015.12.018.
4. Wafti, N.S.A.; Lau, H.L.N.; Loh, S.K.; Aziz, A.A.; Rahman, Z.A.; May, C.Y. Activated carbon from oil palm biomass as potential adsorbent for palm oil mill effluent treatment. *J Oil Palm Res* **2017**, *29*, 278–290, https://doi.org/10.21894/jopr.2017.2902.12.
5. Ahmad-Farid, M.A.; Hassan, M.A.; Roslan, A.M.; Samsudin, M.H.; Mohamad, Z.J.J.; Othman, M.R.; Shirai, Y. Carbon monoxide reduction in the flue gas during biochar production from oil palm empty fruit bunch. *J Clean Prod* **2020**, *258*, https://doi.org/10.1016/j.jclepro.2020.120580.
6. Yasin, N.M.F.M.; Meri, N.H.; Talib, N.; Ghani, W.A.W.A.K.; Rashid, Z.A.; Alias, A.B. Breakthrough

analysis of empty fruit bunch-based hydrogel biochar composite (EFB-HBC) for hydrogen sulphide (H_2S) adsorption study removal. *Adv Eng Res* **2021**, *200*, 216–225, https://doi.org/10.2991/aer.k.201229.030.
7. Lin, C.S.; Ibrahim, N.; Ahmad, N.; Hanif, M.A.; Abdullah, S. Nitric oxide removal by zinc chloride activated oil palm empty fruit bunch fibre. *Malaysian J Fundam Appl Sci* **2021**, *17*, 84–89, https://doi.org/10.11113/mjfas.v17n1.2171.
8. Giles-Jr, H.F.; Wagner, J.R.; Mount, E.M. Design of Experiments. In: *Extrusion.* 2nd ed.; Elsevier: Massachusetts, United States, **2013**; pp. 291–308, https://doi.org/10.1016/B978-081551473-2.50026-X.
9. Montgomery, D.C. *Design and Analysis of Experiments*. 9th ed.; John Wiley & Sons, Inc.: New Jersey, United States. **2017**.
10. Hanif, M.A.; Ibrahim, N.; Md-Isa, K.; Tuan-Abdullah, T.A.; Abdul-Jalil, A. Sulfur dioxide removal by mesoporous silica KCC-1 modified with low- coverage metal nitrates. *Mater Today Proc* **2021**, *47*, 1323-1328, https://doi.org/10.1016/j.matpr.2021.02.807.
11. Chaker, H.; Ameur, N.; Saidi-Bendahou, K.; Djennas, M.; Fourmentin, S. Modeling and Box-Behnken design optimization of photocatalytic parameters for efficient removal of dye by lanthanum-doped mesoporous TiO_2. *J Environ Chem Eng* **2021**, *9*, https://doi.org/10.1016/j.jece.2020.104584.
12. Thommes, M.; Kaneko, K.; Neimark, A.V.; Olivier, J.P.; Rodriguez-Reinoso, F.; Rouquerol, J.; Sing, K.S.W. Physisorption of gases, with special reference to the evaluation of surface area and pore size distribution (IUPAC Technical Report). *Pure Appl Che* **2015**, *87*, 1–19, https://doi.org/10.1515/pac-2014-1117.
13. Ooi, C.H.; Cheah, W.K.; Sim, Y.L.; Pung, S.Y.; Yeoh, F.Y. Conversion and characterization of activated carbon fiber derived from palm empty fruit bunch waste and its kinetic study on urea adsorption. *J Environ Manage* **2017**, *197*, 199–205, https://doi.org/10.1016/j.jenvman.2017.03.083.
14. Liu, X.; He, C.; Yu, X.; Bai, Y.; Ye, L.; Wang, B.; Zhang, L. Net-like porous activated carbon materials from shrimp shell by solution-processed carbonization and H_3PO_4 activation for methylene blue adsorption. *Powder Technol* **2018**, *326*, 181–189, https://doi.org/10.1016/j.powtec.2017.12.034.
15. Mahmood, T.; Ali, R.; Naeem, A.; Hamayun, M.; Aslam, M. Potential of used Camellia sinensis leaves as precursor for activated carbon preparation by chemical activation with H_3PO_4; optimization using response surface methodology. *Process Saf Environ Prot* **2017**, *109*, 548–563, https://doi.org/10.1016/j.psep.2017.04.024.
16. Ahmad, N.; Zahari, F.M.; Ibrahim, N. Influence of hydrogen pre-treatment at different temperatures on copper oxide supported on carbonised oil palm empty fruit bunch (CuO/EFBC) for low-temperature nitric oxide removal. *Waste and Biomass Valorization* **2020**, *11*, 5561–5574, https://doi.org/10.1007/s12649-020-01064-8.
17. Loo, W.W.; Pang, Y.L.; Lim, S.; Wong, K.H.; Lai, C.W.; Abdullah, A.Z. Enhancement of photocatalytic degradation of Malachite Green using iron doped titanium dioxide loaded on oil palm empty fruit bunch-derived activated carbon. *Chemosphere* **2021**, *272*, https://doi.org/10.1016/j.chemosphere.2021.129588.
18. Ibrahim, I.; Tsubota, T.; Hassan, M.A.; Andou, Y. Surface functionalization of biochar from oil palm empty fruit bunch through hydrothermal process. *Processes* **2021**, *9*, https://doi.org/10.3390/pr9010149.
19. Baytar, O.; Ceyhan, A.A.; Şahin, Ö. Production of activated carbon from Elaeagnus angustifolia seeds using H_3PO_4 activator and methylene blue and malachite green adsorption. *Int J Phytoremediation* **2020**, *23*, 693–703, https://doi.org/10.1080/15226514.2020.1849015.
20. Huang, Y.; Li, S.; Chen, J.; Zhang, X.; Chen, Y. Adsorption of Pb(II) on mesoporous activated carbons fabricated from water hyacinth using H_3PO_4 activation: Adsorption capacity, kinetic and isotherm studies. *Appl Surf Sci* **2014**, *293*, 160–168, https://doi.org/10.1016/j.apsusc.2013.12.123.
21. Li, B.; Chunyuan, M. SO_2 removal by powder activated carbon in a drop tube furnace experimental system. *Key Eng Mater* **2018**, *783*, 34–40, https://doi.org/10.4028/www.scientific.net/KEM.783.34.
22. Tailor, R.; Sayari, A. Grafted propyldiethanolamine for selective removal of SO_2 in the presence of CO_2. *Chem Eng J* **2016**, *289*, 142–149, https://doi.org/10.1016/j.cej.2015.12.084.
23. Chen, M.; Deng, X.; He, F. Removal of SO_2 from flue gas using basic aluminum sulfate solution with the byproduct oxidation inhibition by ethylene glycol. *Energy and Fuels* **2016**, *30*, 1183–1191, https://doi.org/10.1021/acs.energyfuels.5b02411.
24. Severa, G.; Head, J.; Bethune, K.; Higgins, S.; Fujise, A. Comparative studies of low concentration SO_2 and NO_2 sorption by activated carbon supported [C_2mim][Ac] and KOH sorbents. *J Environ Chem Eng* **2018**, *6*, 718–727, https://doi.org/10.1016/j.jece.2017.12.020.
25. Xie, P.; Li, C.-L.; Shao, B.; Xu, X.-J.; Chen, X.-D.; Zhao, L.; Zhou, X.; Lee, D.-J.; Ren, N.-Q.; Chen, C. Simultaneous removal of carbon dioxide, sulfur dioxide and nitric oxide in a biofilter system: Optimization operating conditions, removal efficiency and bacterial community. *Chemosphere* **2021**, *276*, https://doi.org/10.1016/j.chemosphere.2021.130084.
26. Hanif, M.A.; Ibrahim, N.; Md Isa, K.; Tuan Abdullah, T.A.; Abdul Jalil, A. Sulfur dioxide removal by mesoporous silica KCC-1 modified with low-coverage metal nitrates. *Materials Today: Proceedings* **2021,** https://doi.org/10.1016/j.matpr.2021.02.807.
27. Lan, H.-C.; Zhang, J.-Y.; Dai, Q.-J.; Ye, H.; Mao, X.-Y.; Wang, Y.-C.; Peng, H.-L.; Du, J.; Huang, K. Highly efficient, selective and reversible capture of sulfur dioxide by methylated-polyethylenimine supported on graphitic carbon nitride. *Chem. Eng. J.* **2021**, *409*, https://doi.org/10.1016/j.cej.2020.127378.

28. Zhang, H.; Niu, J.; Guo, Y.; Cheng, F. Recirculating coking by-products and waste for cost-effective activated carbon (AC) production and its application for treatment of SO2 and wastewater in coke-making plant. *J. Clean. Prod.* **2021**, *280*, https://doi.org/10.1016/j.jclepro.2020.124375.
29. Gani, A.; Wattimena, Y.; Erdiwansyah; Mahidin; Muhibbuddin; Riza, M., Simultaneous sulfur dioxide and mercury removal during low-rank coal combustion by natural zeolite. *Heliyon* **2021**, *7*, https://doi.org/10.1016/j.heliyon.2021.e07052.